NACA RM L55E10a

NATIONAL ADVISORY COMMITTEE FOR AERONAUTICS

RESEARCH MEMORANDUM

EFFECTS OF WING-FUSELAGE FLOW FIELDS ON MISSILE

LOADS AT SUBSONIC SPEEDS

By William J. Alford, Jr.

SUMMARY

333 /4

The flow-field characteristics around a swept-wing airplane model at low subsonic speed are described, and the loads induced on a typical missile model while operating within these flow fields are presented. In addition, theoretical flow fields are compared with experiment and are used in first-order estimations of the resulting induced missile loads.

INTRODUCTION

The loading problems associated with the external storage of tanks, bombs, nacelles, and missiles have become increasingly serious with increase in airspeed, and knowledge of these loads is desirable in the design of the store-supporting members. A study of available data from wind-tunnel tests (refs. 1 to 3), in conjunction with theory (refs. 4 and 5), has indicated that these loads are primarily due to the nonuniform flow field generated by the airplane.

The purpose of this paper is to describe these flow fields at low subsonic speeds and to indicate the magnitude of missile loads that may result because of the nature of these flow fields. In addition, comparisons of theoretical flow fields with experiment are presented. These flow fields, both theoretical and experimental, are used in first-order estimations of the resulting missile loads.

SYMBOLS

α angle of attack, deg

α_l local angle of attack between xy-plane and local flow direction, $\alpha - \epsilon$, deg (see ref. 1)

ϵ angle of downwash, deg

β angle of sideslip

β_l local angle of sideslip between xz-plane and local flow direction, $\beta + \sigma$, deg (see ref. 1)

σ angle of sidewash, deg (see ref. 1)

Λ angle of sweepback, deg

M Mach number

A aspect ratio

λ taper ratio

c local wing chord, ft

x longitudinal distance, ft

y lateral distance, ft

z vertical distance, ft

V_0 free-stream velocity, ft/sec

q_0 free-stream dynamic pressure, lb/sq ft

q_l local dynamic pressure, lb/sq ft

l missile length, ft

b wing span, ft

$\bar{x}$ longitudinal location of chordwise vortices (fig. 8), ft

Γ circulation, sq ft/sec

n chordwise vortex index

m spanwise vortex index

u longitudinal perturbation velocity parallel to free-stream direction (fig. 8), ft/sec

u' perturbation velocity normal to spanwise line of constant sweep, ft/sec

v lateral perturbation velocity normal to free-stream direction (fig. 8), ft/sec

Subscripts:

c/4　　　at quarter chord

c/2　　　at midchord

CG　　　missile center-of-gravity position

TEST CONFIGURATIONS

Presented in figure 1 are configurations used in investigations, made at low speed in the Langley 300 MPH 7- by 10-foot tunnel, in which flow-field surveys were made using the survey rake shown in the center of the figure. This rake consisted of six probes, each of which was instrumented to measure local pitch and sideslip angularities and dynamic pressure. These surveys were made under the fuselage and at each one-quarter semispan location of the swept-wing–fuselage combination and at the one-half semispan location of the unswept-wing–fuselage combination. The range of vertical, spanwise, and chordwise position investigated is indicated by the dots, which represent the leading edge of the survey rake.

Static force and moment measurements were obtained on a typical missile model, shown in the center of figure 2, for various locations within the wing-fuselage flow fields. The range of missile center-of-gravity location investigated is shown by symbols at the data points.

The results of these investigations indicated that the induced longitudinal characteristics were, in general, qualitatively similar for both the swept and unswept configurations, whereas the induced lateral characteristics were considerably more seriously affected for the swept-wing configuration. In view of this result, the discussion deals hereinafter with the swept configuration.

MEASURED FLOW FIELDS

In defining a flow field, or velocity distribution, it is necessary to know both the direction and magnitude of the local velocity vectors. For convenience, the flow directions are expressed as vertical and lateral inclinations and the magnitudes are expressed as dynamic pressure.

The local angles of attack as measured about the one-half semispan location of the swept-wing–fuselage combination are presented in figure 3. The conditions depicted, which are for an angle of attack of 8° and zero sideslip, are equivalent to the 6g service load limit of a typical fighter
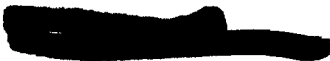
airplane for a velocity of 430 mph at an altitude of 20,000 feet. These data are presented in contour form; that is, as lines of constant angularity for the physical space surrounding the airfoil profile. The missile outline is superimposed on the contours to show its size relative to the local wing chord and to indicate the angularity gradients to which it is subjected. Regions where the local angles are greater than 8° indicate an upflow and regions where these angles are less than 8° are indicative of downflow. The angularity variation along the center line of the missile, which in this case was 15 percent of the local wing chord below the wing chord plane, is presented in the lower portion of figure 3. Two missile center-of-gravity locations are shown to indicate both the angularity magnitudes and the angularity gradient that exist along the missile center line. For the chordwise range indicated, the local angles of attack vary from 5° to 12°, a gradient of 7° along the missile center line extended.

Presented in figure 4, for the same vertical plane, are the local sideslip angles. It should be noted that the perturbation velocities which generate these lateral angularities are in a plane normal to the plane of the figure. The local sideslip angles below the wing chord plane represent an outflow direction (toward the wing tip), and the angles above the chord plane indicate an inflow (toward the plane of symmetry). The sideslip angles that exist along the missile center line are presented in the lower graph and indicate a gradient of 6° along the center line extended. Comparison of these sideslip gradients with angle-of-attack gradients of figure 3 shows that they are of the same magnitude and could be considerably more important since the supporting pylon would have its least structural strength in the lateral direction.

The local dynamic pressures referenced to free-stream conditions are presented in figure 5. The effects of the induced longitudinal velocities are as would be expected, since the dynamic pressures are increased above and decreased below the wing chord plane. Sizable gradients are again in evidence over the length of the missile center line extended. These data also indicate that, for positive angles of attack, the dynamic pressure can effect load reductions but, for negative angles of attack, would cause large load increases.

MEASURED MISSILE LOADS

The preceding discussion has attempted to define and illustrate the flow phenomenon existing around the airplane. Having shown that the missile is forced to operate in regions of adverse flow, it would be desirable to correlate the flow characteristics with the loads induced on the missile.
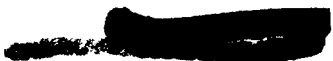
The total missile normal forces, in pounds, for a free-stream dynamic pressure of 445 pounds per square foot are presented in figure 6. These data were obtained by assuming a full-scale missile to be stored externally on a typical fighter airplane at a velocity of 430 mph at an altitude of 20,000 feet. The effects of compressibility are absent since the missile loads data were obtained at low speed. The normal-force load center, in percent of the missile length from the missile nose, is also presented. These parameters are given for various locations of the missile center of gravity in fractions of the local wing chord, relative to the leading edge of the local wing chord. For comparison, the isolated-missile character-istics, at an identical attitude, are shown by the dashed lines. The two missile center-of-gravity locations (fig. 6) indicated by the solid sym-bols are identical to those shown in the lower graph of figure 3. It should be noted that the total normal forces are a result of an integra-tion of the angularities (fig. 3) and dynamic pressures (fig. 5) over the length of the missile. Considering the rearward location of the missile center of gravity ($x/c \approx 0.45$), the missile is seen to be operating in a region of reduced angularity and consequently experiences a reduced normal force when compared to the isolated missile. Further examination shows that the tail is operating in a slightly higher angular region than the missile wing (fig. 3) and consequently the load center is drawn aft. When the missile center of gravity is in the forward position ($x/c \approx -0.75$), the missile is experiencing higher angularities (fig. 3) and the resulting normal forces are considerably increased (fig. 6). For the range of mis-sile center-of-gravity location investigated, the normal forces are ini-tially decreased approximately 30 percent and later increased about 50 per-cent with a total load-center travel of approximately 10 percent of the missile length.

Presented in figure 7 are the total missile side forces and side-force load centers as a function of missile center-of-gravity location. Recalling that the airplane-missile combination is at zero sideslip, the comparable isolated-missile characteristics would be zero. In order to show the relative magnitude of these side loads, the isolated-missile characteristics at 6° sideslip are shown as the dashed lines. Once again the solid symbols represent the missile center-of-gravity locations shown in the lower graph of figure 4. Since the missile was below the wing, the local sideslip angles are in an outward direction (fig. 4) and cause neg-ative side forces (force directed toward the wing tip, fig. 7). The side loads and load centers are as would be expected since, when the missile wings are in the highest angular region (fig. 4, $x/c \approx 0.50$), the load center moves forward (fig. 7) and when the tail is in the highest angular region ($x/c \approx -0.75$) the load center moves rearward with a total load-center travel of 30 percent missile length for the chordwise range indi-cated. The region of greatest side load is encountered when the missile wings are in the highest angular region.

THEORETICAL FLOW FIELDS

Once a problem has been defined and shown to exist, it then becomes desirable to have, or to formulate, procedures by which the individual components of the system can be studied.

In the present instance, the chief difficulty appears to be in the severe angular gradients that are generated by the airplane. The mathematical models used to calculate these flow fields assumed a simulated lifting surface (fig. 8), the appropriate airfoil-section singularity distribution (by method of reference 6), and simple sweep theory (fig. 8). The simulated lifting surface, shown in figure 8, approximated both the spanwise and chordwise distributions of vorticity by discrete horseshoe vortices. The spanwise vorticity distribution was represented by 10 horseshoe vortices and the chordwise distribution was represented by four vortices of equal strength, the chordwise locations of which were determined from the familiar two-dimensional circulation distribution shown in figure 8. The nonlifting (thickness) effects were determined from the source-sink distribution that satisfied the two-dimensional airfoil-section boundary conditions (ref. 6) and were corrected by simple sweep theory (fig. 8) to account for wing sweep.

Typical results of these calculations compared with experiment are presented in figures 9 and 10. Figure 9 presents the local angles of attack and figure 10 presents the local angles of sideslip for the one-half semispan location $\left(y\middle/\frac{b}{2} = 0.5\right)$ of the swept-wing–fuselage combination. The experimental data are shown as the symbols and the theory is shown as the solid-line curves. As is seen, the agreement is poor for $\alpha = -8^\circ$. This disagreement is presumed to be due to the fact that the flow on the suction side of the airfoil assumes characteristics that are nonpotential. The agreement is good between theory and experiment (figs. 9 and 10) for $\alpha = 0^\circ$ and for all positive angles of attack up to $\alpha = 24^\circ$, where theory then overestimates the local angles of attack. This is rather surprising from consideration of the nonpotential nature of the flow on the suction side of the wing surface. Calculations made for the three-quarter semispan location have shown that theoretical values obtained by using the theoretical span-load distribution overestimate the experimental values.

ESTIMATED MISSILE LOADS

With the flow-field characteristics known, the next step is to use them, in conjunction with the missile component characteristics, to estimate the airplane induced missile loads. This estimate has been made and figures 11 and 12 present sample comparisons of theory and experiment.
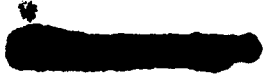
Presented in figure 11 are the estimated normal forces and normal-force load centers. Experimental loads are again represented by the symbols. The estimation obtained by using the experimental flow fields is shown as the solid curves and the estimation by using the theoretical flow fields is shown as the dashed curves. Good agreement in estimating the normal forces is obtained by both estimates over the rear portion of the chord, with evidence that theory gives values too low ahead of the leading edge. The load centers are also seen to be well predicted.

In the case of the estimated side forces (fig. 12) both estimates are low, although the side-force load centers are well predicted. The reason for the lack of agreement for the side forces is not completely understood.

The data that have been presented were obtained at low speed in order to permit convenient examination of the nature of the complex flow that exists around airplanes. The use of a missile as the store configuration was for illustrative purposes, and the approach utilized should be equally valid for other external stores, although such application has not, at present, been adequately demonstrated.

The results of a brief theoretical study have indicated that the effects of compressibility, for subcritical Mach numbers, are to generate larger flow distortions and consequently larger induced missile loads, although the flow structure remains similar to that of an incompressible nature.

CONCLUDING REMARKS

In summary, these results have shown that the flow fields in regions beneath the one-half semispan location of a swept-wing airplane model can be calculated. These flow fields can then be used in first-order estimations of the loads experienced by a missile while operating in these flow fields.

Langley Aeronautical Laboratory,
    National Advisory Committee for Aeronautics,
        Langley Field, Va., April 25, 1955.

NACA RM L55E10a

REFERENCES

1. Alford, William J., Jr., Silvers, H. Norman, and King, Thomas J., Jr.:
   Preliminary Low-Speed Wind-Tunnel Investigation of Some Aspects of
   the Aerodynamic Problems Associated With Missiles Carried Externally
   in Positions Near Airplane Wings. NACA RM L54J20, 1954.

2. Alford, William J., Jr., Silvers, H. Norman, and King, Thomas J., Jr.:
   Experimental Aerodynamic Forces and Moments at Low Speed of a Missile
   Model During Simulated Launching From the Midsemispan Location of a
   45° Sweptback Wing-Fuselage Combination. NACA RM L54K11a, 1954.

3. Alford, William J., Jr.: Experimental Static Aerodynamic Forces and
   Moments at Low Speed on a Canard Missile During Simulated Launching
   From the Midsemispan and Wing-Tip Locations of a 45° Sweptback Wing-
   Fuselage Combination. NACA RM L55A12, 1955.

4. Luce, R. W., Jr., and Velton, E. J.: Investigation of the Aerodynamic
   Interference of a Launching Aircraft on the Sparrow II Missile.
   Rep. No. SM-14383 (Bur. Aero. Contract NOa(s)51-252), Douglas Aircraft
   Co., Inc., Oct. 29, 1952.

5. Evans, K. E., and Freeman, P. A.: Launch Study Supplement XAAM-N-4
   (Oriole) Launching Dispersions Including the Effects of the Airplane
   Wing and Pylon on the Flow Field Around the Missile. Eng. Rep.
   No. 5058 (Contract NOa(s)51-194-C), The Glenn L. Martin Co.,
   Apr. 1952.

6. Smith, R. H.: Aerodynamic Theory and Test of Strut Forms - I. NACA
   Rep. 311, 1929.
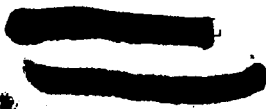
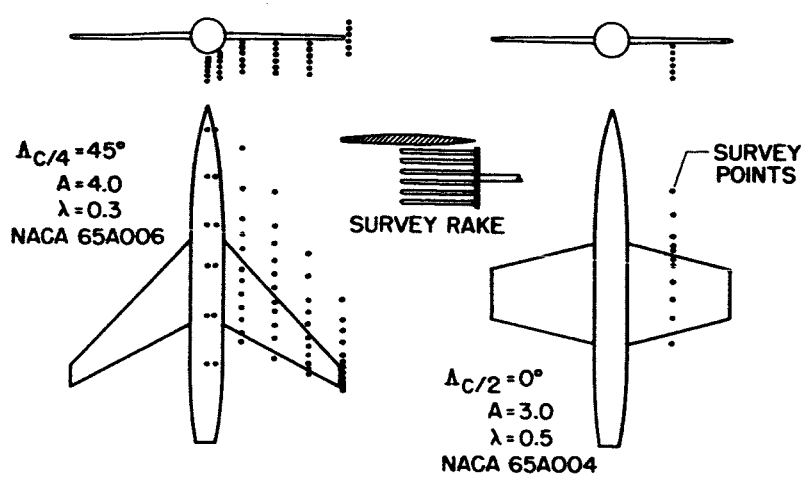FLOW-FIELD-SURVEY CONFIGURATIONS

$\alpha = -8°$ TO $24°$; M=0.13

$\Lambda_{C/4} = 45°$
A=4.0
λ=0.3
NACA 65A006

SURVEY RAKE

SURVEY POINTS

$\Lambda_{C/2} = 0°$
A=3.0
λ=0.5
NACA 65A004

Figure 1

MISSILE-LOADS CONFIGURATIONS

$\alpha = -8°$ TO $20°$; M=0.13

Figure 2

LONGITUDINAL-ANGULARITY FIELD

$\alpha = 8°; \ \beta = 0°$

Figure 3

LATERAL-ANGULARITY FIELD

$\alpha = 8°; \ \beta = 0°$

Figure 4

DYNAMIC-PRESSURE FIELD

$\alpha = 8°; \beta = 0°$

Figure 5

NORMAL FORCES

$\alpha = 8°; \beta = 0°; q_0 = 445$ LB/SQ FT

Figure 6

SIDE FORCES

$\alpha = 8°; \quad \beta = 0°; \quad q_0 = 445 \text{ LB/SQ FT}$

Figure 7

THEORETICAL FLOW-FIELD MODELS

LIFTING SURFACE   THICKNESS-SWEEP

n	$\bar{x}/c$
1	.01
2	.09
3	.27
4	.62

$$\beta_l = \text{TAN}^{-1}\left(\frac{u' \sin \Lambda}{V_0 + u' \cos \Lambda}\right)$$
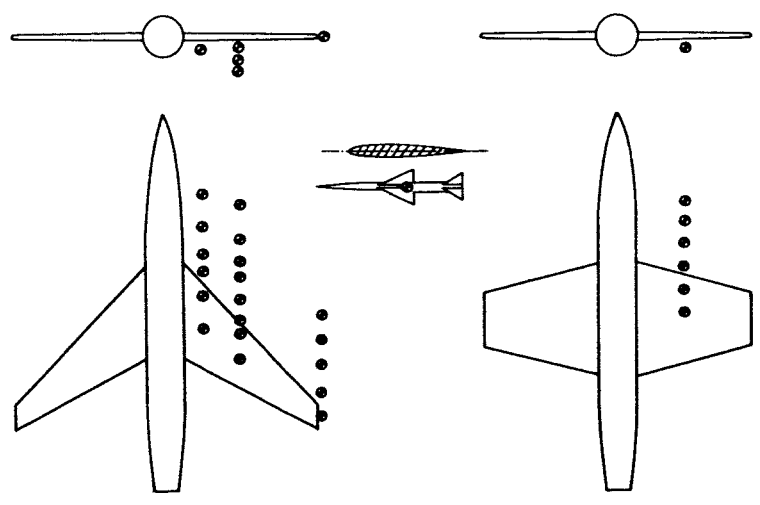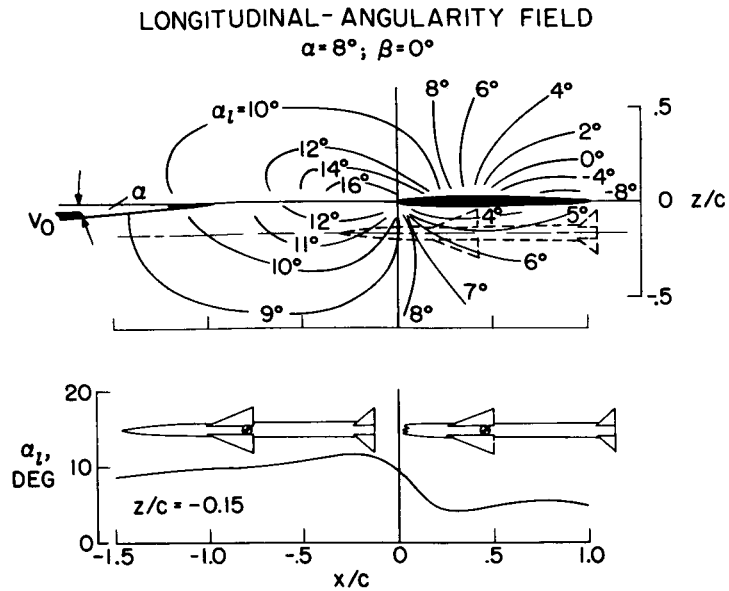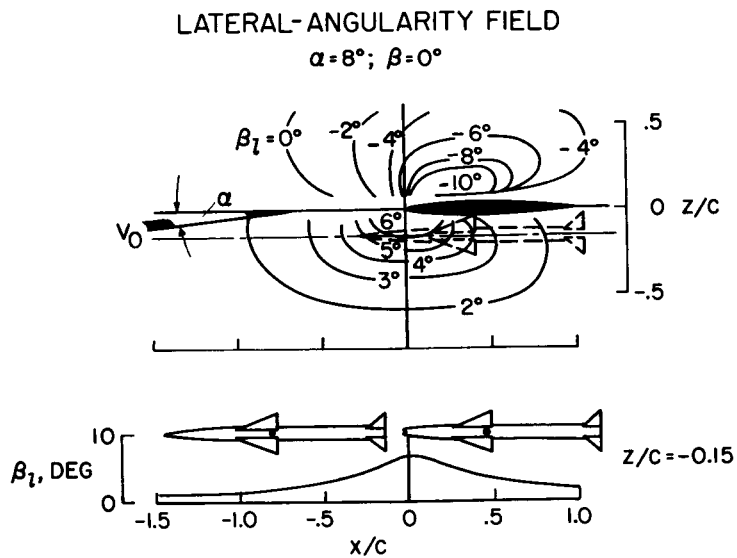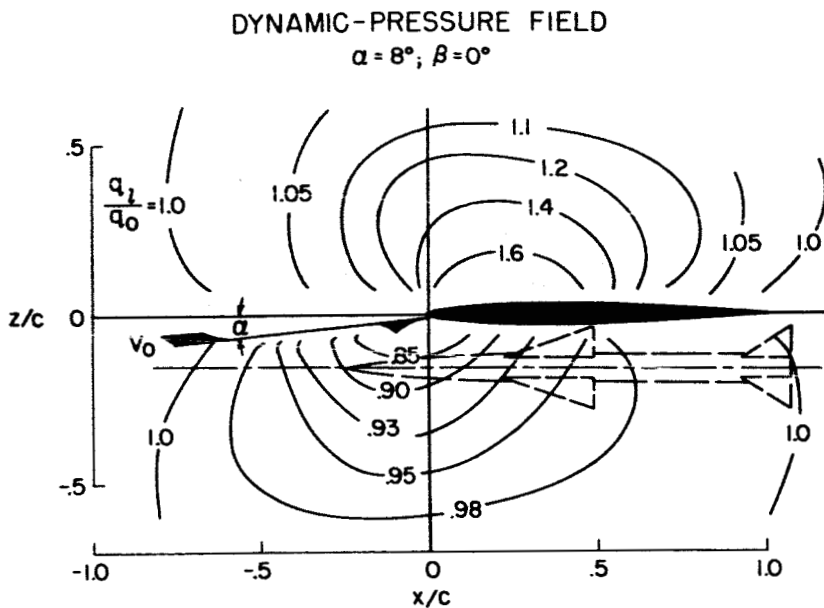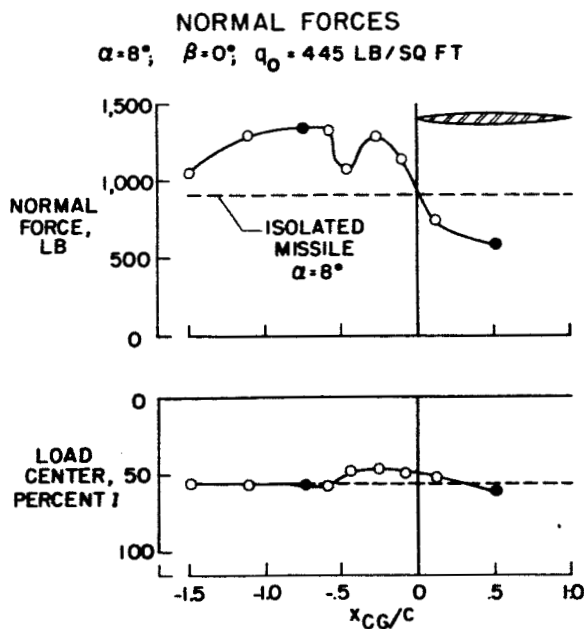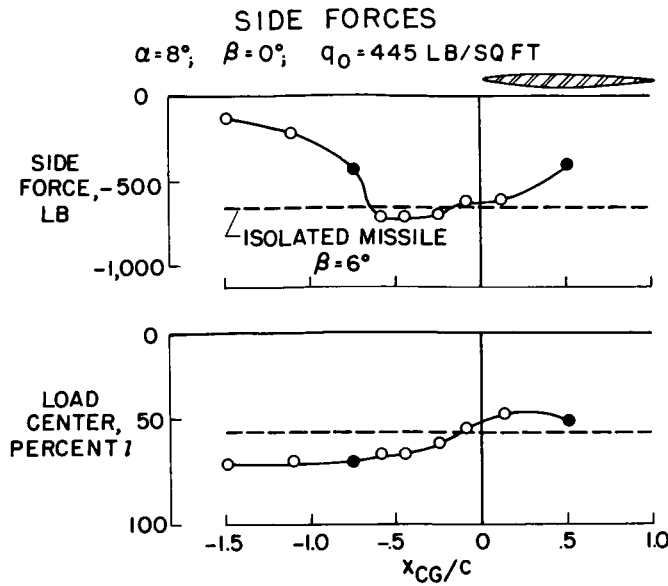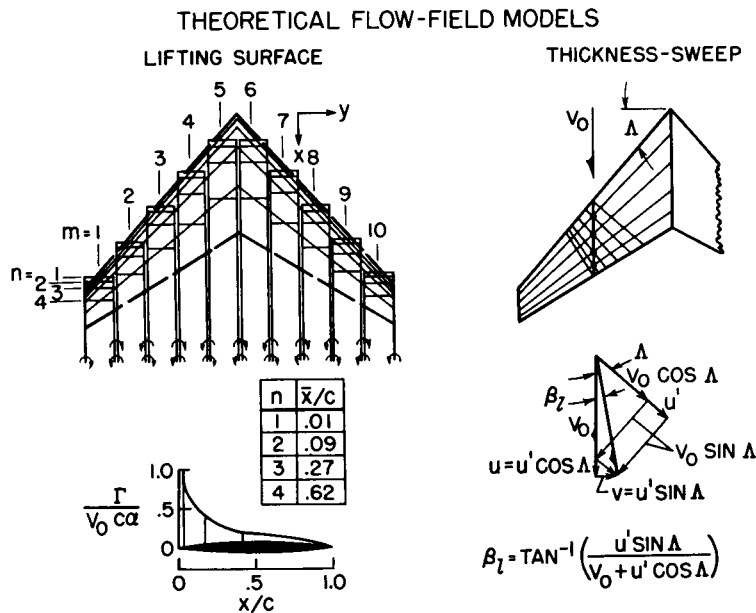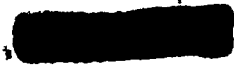
Figure 8

PREDICTION OF LONGITUDINAL ANGULARITIES
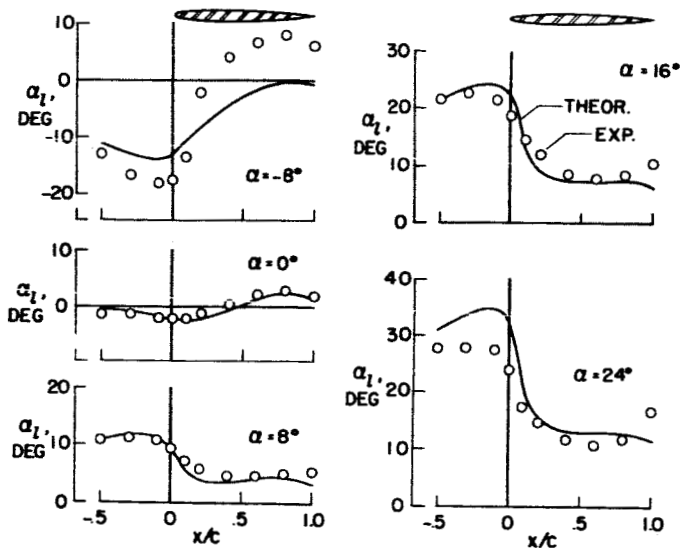
$\frac{y}{b/2} = 0.5$;　$z/c = -0.15$

Figure 9

PREDICTION OF LATERAL ANGULARITIES
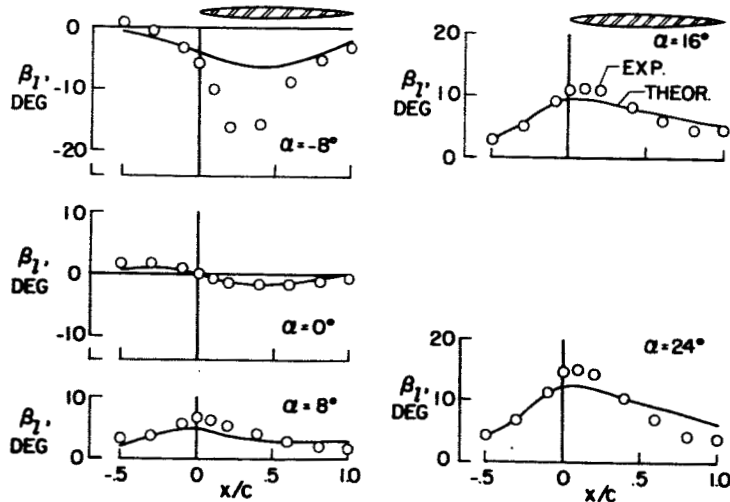
$\frac{y}{b/2} = 0.5$;　$z/c = -0.15$;　$\beta = 0°$

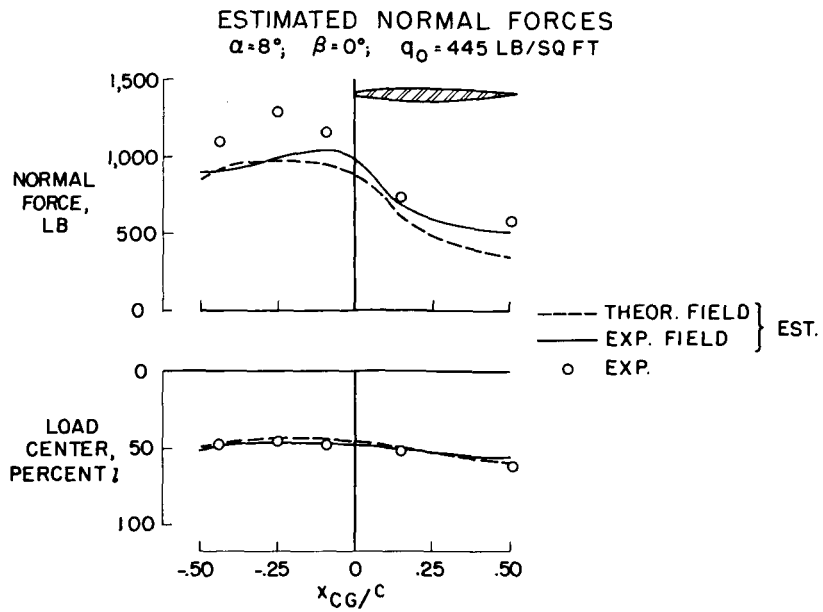Figure 10

ESTIMATED NORMAL FORCES

$\alpha = 8°;$ $\beta = 0°;$ $q_0 = 445$ LB/SQ FT

Figure 11

ESTIMATED SIDE FORCES

$\alpha = 8°;$ $\beta = 0°;$ $q_0 = 445$ LB/SQ FT

Figure 12